Accepted Manuscript online: 2022-11-04 Article published online: 2023-01-27

Broadly Applicable Synthesis of Heteroarylated Dithieno[3,2-*b*:2′,3′-*d*]pyrroles for Advanced Organic Materials – Part 1: Conducting Electropolymers

Christoph Lorenz[a]
Astrid Vogt[a]
Judith Millan[b]
Elena Mena-Osteritz[a]
Peter Bäuerle* [a]

[a] Institute of Organic Chemistry II and Advanced Materials, University of Ulm, Albert-Einstein-Allee 11, 89081 Ulm, Germany
[b] Dpto. de Química – Facultad de Ciencia y Tecnología, Universidad de la Rioja, Madre de Dios, 53, 26006 Logroño-La Rioja, España
* peter.baeuerle@uni-ulm.de

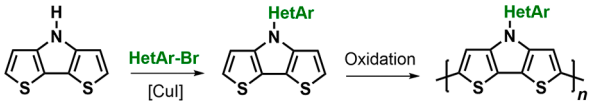

Received: 12.08.2022
Accepted after revision: 27.10.2022
DOI: 10.1055/a-1972-5895; Art ID: OM-2022-08-0031-OA

Abstract Herein, a novel and versatile method for the synthesis of N-heteroarylated dithieno[3,2-*b*:2,3′-*d*]pyrroles (DTPs) is reported. By microwave-assisted Cu-catalyzed coupling of parent *H*-DTP **1** with 5- and 6-membered heteroaromatic halides, a variety of novel N-functionalized DTPs were obtained. Supported by quantum chemical calculations and X-ray structure analysis, structural and optoelectronic properties of the π-conjugated systems were investigated and led to valuable structure–property relationships. Selected derivatives were electropolymerized to corresponding conducting DTP polymers.

Key words: organic materials, conjugated molecules, dithienopyrrole, Cu-catalyzed C – N coupling, optoelectronic properties, quantum chemical calculations, electropolymerization, poly(dithienopyrrole)

Introduction

Functionalized dithieno[3,2-*b*:2′,3′-*d*]pyrroles (DTPs) are frequently implemented as electron-rich units in semiconducting materials for organic electronic devices.[1–3] The typically used *N*-alkyl and *N*-aryl DTPs are efficiently synthesized by Pd-catalyzed Buchwald–Hartwig amination of halogenated bithiophene precursors and alkyl or aryl amines with the formation of the central pyrrole ring.[3,4] However, DTPs bearing directly connected heteroaromatic substituents at the central nitrogen were not described using this general approach. For example, we have tried to react 3,3′-dibromo-2,2′-bithiophene with heteroaromatic 2-aminothiazole. Neither with palladium nor with copper catalysis, any conversion to the targeted thiazolyl-DTP was observed.[5]

A further drawback of this approach is the limited availability of amino-substituted heterocycles such as, e.g., 2- or 3-aminothiophenes as amino components in this C – N coupling reaction due to their inherent instability.[6] In that respect, the first and only N-heteroarylated DTP was recently published by Tang et al., who reacted parent *H*-DTP, which can be conveniently synthesized on a larger scale,[7] with 2-iodo-5-hexylthiophene in a copper-catalyzed variant of the Ullmann reaction to receive N-(2-thienyl)-substituted DTP in 50% yield.[8] This DTP was used as a central part of a larger co-oligomer, which served as a hole-transport layer in perovskite solar cells.[9] On these grounds, it becomes evident that there is a requirement to expand the family of N-heteroarylated DTPs.

We have very recently disclosed a straightforward and viable 'inverted' method for the preparation of a series of N-arylated DTPs by Pd- or Cu-catalyzed coupling of parent *H*-DTP **1** as the amine component with widely available aryl and acene bromides.[10] Herein, we now describe microwave-assisted Cu-catalyzed heteroarylation reactions of *H*-DTP **1** with well available 5- and 6-membered heteroaromatic halides leading to a series of novel N-heteroarylated DTPs **3a**–**3n** (Scheme 1). Eventually, selected N-heteroarylated DTPs **3** were electropolymerized to the corresponding conducting DTP-polymers **P3**.

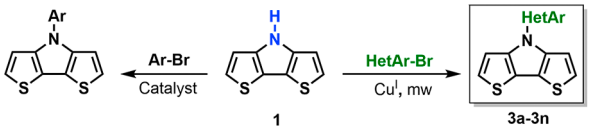

Scheme 1 N-Arylation reactions of *H*-DTP **1** (left, previous work, ref. 10) and microwave-assisted, Cu-catalyzed heteroarylation of *H*-DTP **1** to yield novel N-heteroarylated DTPs **3a–3n** (right, this work).

Results and Discussion

Synthesis of N-Heteroarylated DTPs

For the N-arylation reaction of *H*-DTP **1** with aryl and acene bromides, it turned out that besides Pd-catalysis, also copper iodide (CuI) under microwave irradiation delivered good yields of some N-aryl DTPs, however with a varying substrate spectrum.[10] Because the reaction of *H*-DTP **1** with heterocyclic 3-bromothiophene **2a** and $Pd(OAc)_2/P(t\text{-}Bu)_3$ as a catalytic system gave N-(3′-thienyl)-substituted DTP **3a** in only 4% yield,[5] we alternatively tested the microwave-assisted, ligand-free Cu(I)-catalyzed method, which was previously described for the reaction of the more robust analogue 9*H*-carbazole with aryl and heteroaryl bromides or iodides.[11] A screening of these reaction conditions for the reaction of the more electron-rich *H*-DTP **1** with differently halogenated thiophenes, various copper sources, bases, and additives revealed that the highest product formation of DTP **3a** (77%) was achieved with 3-bromo- and equally with 3-iodothiophene, with 10 mol% CuI as a catalyst and Cs_2CO_3 as a base in DMF at 160 °C under microwave irradiation for 45 min (Table 1).

Table 1 Microwave-assisted synthesis of 3′-thienyl-substituted DTP **3a** via Buchwald–Hartwig amination of *H*-DTP **1** and 3-thienyl halides **2a–c**

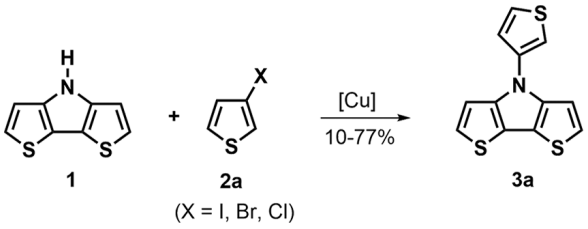

Entry	X	Catalyst	Base	Additive	Temp [°C]	Yield [%]
1	Cl	CuI	Cs_2CO_3	–	180	10
2	Br	CuI	Cs_2CO_3	–	140	65
3	Br	CuI	NaO*t*Bu	–	160	76
4	Br	CuI	Cs_2CO_3	–	160	77[a]
5	Br	CuI	Cs_2CO_3	DMEDA	160	63[b]
6	Br	CuI	Cs_2CO_3	H_2O	160	60[c]
7	Br	$Cu(OAc)_2$	Cs_2CO_3	–	160	65
8	Br	CuBr	Cs_2CO_3	–	140	57
9	I	CuI	Cs_2CO_3	–	160	77

[a]The reaction was also carried out in a Schlenk flask for 16 h instead in a microwave vial and 67% yield was obtained; [b]0.4 eq. DMEDA; [c]250 µL H_2O.

Having established these frame conditions, we examined the scope of this DTP-heteroarylation and reacted *H*-DTP **1** with in total fourteen 5- and 6-membered heterocyclic bromides comprising different electronic characters and reactivities. The results are summarized in Table 2. The reaction using isomeric 2-bromothiophene **2b** gave 2′-thienyl-DTP **3b** in 58% yield. Furthermore, we could introduce 2′-furyl (**3c**), 3′-furyl (**3d**), 2′-selenophenyl (**3e**), and 1,3-thiazol-2′-yl (**3g**) substituents to the DTP core in similar good yields (48–68%), whereby the oxidation-sensitive *N*-methylpyrrol-2′-yl-DTP (**3f**) was formed in a lower 27% yield. Extended substituents were also tested by using bithien-5′-yl, benzo[*b*]thien-2′-yl, and benzo[*b*]fur-2′-yl resulting in heteroaryls **3h, 3i**, and **3j** in yields of 43–46%.

According to the results obtained for the 5-membered heterocycles, we also tested the electron-deficient 6-membered bromopyridines **2k–l** and bromopyrimidines **2m–n.** In that respect, pyridyl and pyrimidyl-substituted DTPs **3k–n** were obtained in moderate to good yields (26–82%) when a higher temperature of 180 °C was applied. Due to the electron-withdrawing effect of the respective heterocycle at the DTP-nitrogen, the products seem to be better stabilized against oxidation and decomposition by follow-up reactions. The chemical structures of all prepared heteroarylated DTPs **3a–n** were fully characterized and their purity and structures confirmed by HPLC, NMR spectroscopy, and mass spectrometry (GC-MS, HRMS), respectively.

Single Crystal X-Ray Structure Analysis of 3-Thienyl-DTP 3a

Single crystals of 3′-thienyl-substituted DTP **3a** were obtained by slow evaporation of a THF solution to afford yellowish trapezoid-shaped crystals suitable for X-ray structure analysis. DTP **3a** crystallized in the monoclinic centrosymmetric space group $P2_1/n$ with two molecules (M1 and M2) in the asymmetric unit with a unit cell (a = 9.34338 (14) Å, b = 8.42876(13) Å, c = 27.7728(5) Å, a = 90°, b = 96.5304(17)°, g = 90°, V = 2173.00(6) Å^3) containing eight molecules in total (Table S1, Supporting Information, SI). The molecular geometry of the asymmetric unit of DTP **3a** is shown in Figure 1 (left) and Figure S1 (SI), and selected bond lengths, bond angles, and torsion angles are summarized in Tables S2–S4 (SI). The bond lengths and angles in the central DTP unit are quite typical and correspond to fused heteroacenes with reduced bond length alternation.[12] Torsion angles of 27.4° and 32.8° for the 3′-thienyl substituent versus the DTP plane were determined and are slightly smaller than the torsion angle obtained for *N*-phenyl-DTP **3o** (37°).[13]

Table 2 N-Heteroarylation reaction of *H*-DTP **1** with bromides **2a–n** to N-heteroarylated DTPs **3a–n**[a]

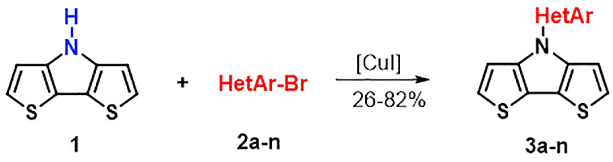

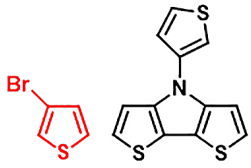

2a/3a (77%)

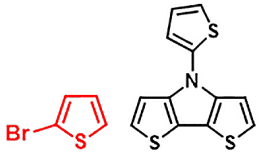

2b/3b (58%)

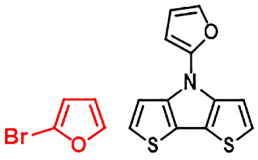

2c/3c (52%)

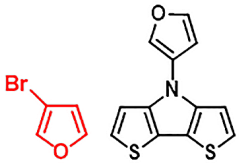

2d/3d (68%)

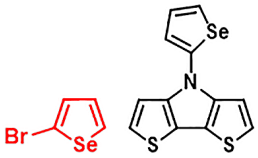

2e/3e (49%)

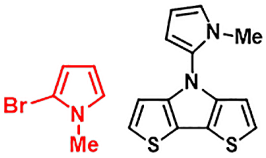

2f/3f (27%)

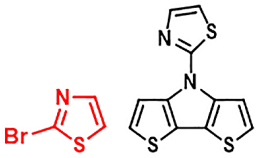

2g/3g (48%)

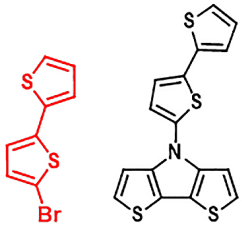

2h/3h (46%)

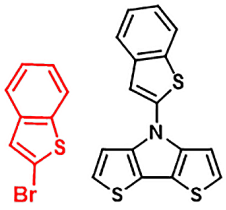

2i/3i (43%)

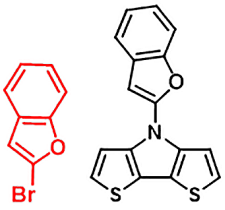

2j/3j (44%)

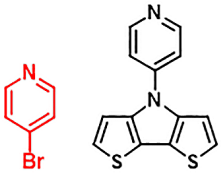

2k/3k (27%)

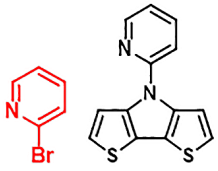

2l/3l (26%)

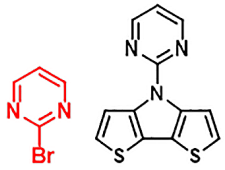

2m/3m (82%)

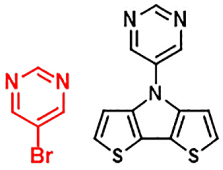

2n/3n (40%)

[a]Yields are given as isolated yields. Reaction conditions: *H*-DTP **1** (1 equiv), heteroaryl bromide **2a–n** (1.1 equiv), CuI (10 mol%), base (1.2 equiv), DMF (2 mL), sealed microwave vial (300 W, 15 bar, 160 – 180 °C, 45 min).

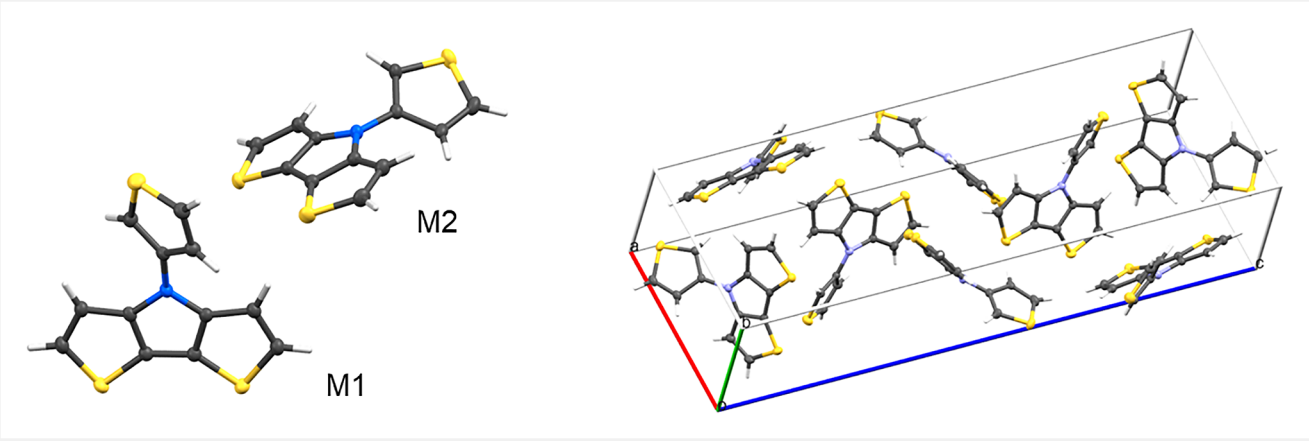

Figure 1 Single-crystal X-ray structure analysis of 3′-thienyl-DTP **3a**: the asymmetric unit composed by two molecules (left) and the unit cell containing eight molecules. For clarity, only one of the two disordered forms (*cis–trans* isomerization at the 3′-thienyl substituent) is shown. Ellipsoids for non-hydrogen atoms are set at 50% probability.

The packing motif of DTP-derivative **3a** includes a dimeric arrangement of one of the molecules (M2) in the asymmetric unit (Figure S2b, SI), which shows several H–S and H–C non-bonding interactions smaller than the sum of the van der Waals radii. The M2-molecules in the dimer show π–π stacking at distances of 3.29 Å. Molecules M1 arrange in a herringbone fashion to each other (Figure S2a, SI) and interact with M2-dimers (Figure S2c, SI) through H–S and H–C intermolecular interactions (Table S5). Intramolecular interactions (Figure S3, Table S6, SI) in each of the molecule M1 and M2 occur between the α- and β-C atoms of the thienyl substituent and C-atoms of the DTP unit forced by the twisting of the substituent with respect to the DTP backbone. The latter effect should be attributed to packing effects in the crystal.

Optical and Redox Properties of DTP-Derivatives 3a–3o

Optical investigations of the N-heteroarylated DTP **3a–n** were performed using UV-vis absorption spectra in THF. Exemplarily, UV-vis spectra of DTPs **3b** (2′-thienyl), **3h** (5′-bithienyl), and **3i** (2′-benzothienyl) are shown in Figure 2 (left); all data are compiled in Table 3. The UV-vis spectra of the heteroarylated DTPs **3a–3g** and **3k–3n** are dominated by a main absorption band in the UV-regime around 294 to 315 nm which we address to the π–π* transition of the central DTP unit. In most cases, these bands are vibronically split with extinction coefficients ranging from around 19 000 $M^{-1}\cdot cm^{-1}$ to 40 000 $M^{-1}\cdot cm^{-1}$. The largest red-shift of this absorption band compared to parent *N*-phenyl DTP **3o**

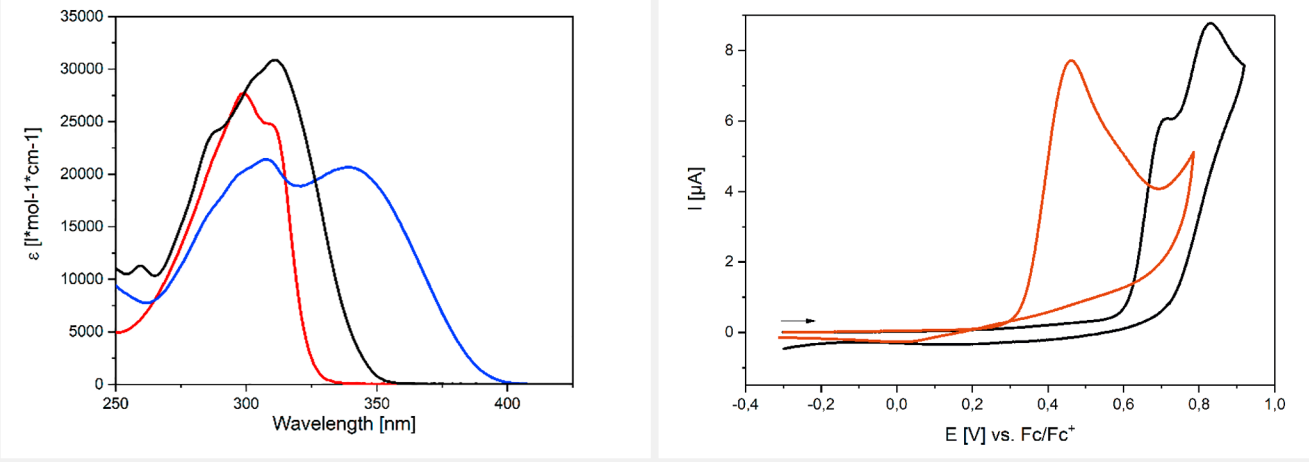

Figure 2 UV-vis absorption spectra of N-heteroarylated DTP **3b** (red curve), **3h** (blue), and **3i** (black) in THF solution (left). Cyclic voltammograms of 2′-pyrrolyl-DTP **3f** (red curve) and 5′-pyrimidyl-DTP **3n** (black) in dichloromethane/acetonitrile (1 : 1)/tetrabutylammonium hexafluorophosphate (0.1 M), 100 mV/s, r.t., potentials vs. ferrocene/ferricenium (Fc/Fc^+).

Table 3 Optical and redox data of heteroarylated DTPs **3a–3n**

DTP	R	λ_{abs} [nm][a]	ε [$M^{-1} \cdot cm^{-1}$]	E_g^{opt} [eV][b]	E_p^{Ox1} [V][c]	E_p^{Ox2} [V][c]	E_{onset} [V][c]	HOMO [eV][d]	LUMO [eV][e]
3a	3′-Th	299 (309)	27 710	3.85	0.63	–	0.59	−5.69	−1.84
3b	2′-Th	299 (309)	27 100	3.84	0.68	–	0.64	−5.74	−1.90
3c	2′-Fu	297 (306)	26 215	3.76	0.65	–	0.62	−5.72	−1.96
3d	3′-Fu	297 (308)	24 420	3.85	0.64	–	0.61	−5.71	−1.86
3e	2′-Se	(301) 309	23 470	3.68	0.70	–	0.66	−5.76	−2.08
3f	2′-Pyr	294 (306)	22 830	3.91	0.46	–	0.42	−5.52	−1.61
3g	2′-Thia	270, 315 (325)	31 900	3.69	0.71	–	0.67	−5.77	−2.08
3h	5′-Bith	307, 339	21 430	3.19	0.55	–	0.52	−5.62	−2.43
3i	2′-BTh	259, (289) 311	30 870	3.61	0.69	0.87	0.66	−5.76	−2.15
3j	2′-BFu	270, 310	31 400	3.58	0.72	–	0.68	−5.78	−2.20
3k	4′-Pyrid	304 (312)	19 150	3.78	0.69[f]	0.87	0.82	−5.92	−2.14
3l	2′-Pyrid	307 (314)	30 670	3.77	0.63	0.83	0.59	−5.69	−1.92
3m	2′-Pyrim	303	39 240	3.69	0.66	–	0.60	−5.70	−2.01
3n	5′-Pyrim	301	24 180	3.74	0.72[f]	0.83	0.68	−5.78	−2.04
3o[g]	Ph	299	28 400	3.86	0.60	–	0.50	−5.70	−1.84

[a]UV-vis spectra were measured in THF, maxima underlined, shoulders in brackets. [b]Calculated from the onset value of the longest wavelength band by $E_g = 1240/\lambda_{onset}$. [c]Cyclic voltammograms measured in DCM or DCM : ACN 1 : 1/tetrabutylammonium hexafluorophosphate (0.1 M), 100 $mV \cdot s^{-1}$, potentials referenced against the ferrocene/ferricenium couple (Fc/Fc^+). [d]Calculated from the onset value of the oxidation wave; Fc/Fc^+ was set to −5.1 eV vs. vacuum. [e]Calculated by taking the optical gap into account ($E_{HOMO} - E_g^{opt}$). [f]Peak, which vanishes after the 2nd or 3rd scan. [g]Values from ref. 5.

is noted for thiazolyl derivative **3g** ($\Delta\lambda_{max} = 1699\ cm^{-1}$), and we assume that charge-transfer (CT) from the DTP-donor to the electron-withdrawing thiazolyl substituent contributes to this transition. In the case of DTP **3h**, a second absorption band at lower energies becomes visible and corresponds to the π–π* transition of the bithiophene substituent (Figure 2, left). The optical energy gaps, which were determined from the onset value of the longest wavelength band, are in the range of $E_g = 3.58 - 3.91$ eV, which are close to the value for the parent phenyl-DTP **3o** ($E_g = 3.86$ eV). Only bithiophene-DTP **3h** exhibits a significant lower energy gap of 3.19 eV, related to the dissimilar character of the low-energy band in comparison to the rest of the compounds.

The redox properties of the DTP-derivatives **3a–3n** were studied by CV in dry dichloromethane (DCM) or DCM/acetonitrile (ACN) 1 : 1 mixtures with tetrabutylammonium hexafluorophosphate (TBAHFP; 0.1 M) as the supporting electrolyte and potentials were referenced against the ferrocene/ferricenium (Fc/Fc^+) couple (Table 3). The electrochemical characterization of the DTPs **3a–3n** expectedly revealed irreversible (one-electron) oxidation waves in the CV which we address to the oxidation of the basic DTP units. Due to their reactive α-positions, the formed radical cations undergo follow-up reactions and couple to larger entities such as conjugated polymers (vide infra). For the majority of the derivatives, the peak potentials are more positive compared to reference *Ph*-DTP **3o** ($E_p^a = 0.60$ V) and vary in the limited range of 0.63 V for the rather electron-rich thienyl and furyl-derivatives to 0.72 V for DTPs with electron-deficient substituents such as thiazolyl (**3g**), benzofuryl (**3j**), and pyrimidyl (**3n**). This indicates that the oxidation of the DTP unit is only insignificantly influenced by electronic effects of the substituent (Figure 2, right). Exceptions are noted by electron-rich pyrrolyl-DTP **3f** and bithienyl-DTP **3h**, which are oxidized at lower potential ($E_p^a = 0.46$ V and 0.55 V) than reference *Ph*-DTP **3o**. We assume that in the latter cases the oxidation and formation of radical cations can be attributed to the substituents.[14]

These findings are in agreement with computational results showing that in the HOMOs no electron density is found at the DTP-nitrogen suppressing distinct electron interaction of the substituent with the DTP core (vide infra).[5] Furthermore, HOMO energies were calculated from the onset potential of the oxidation wave ranging from −5.52 eV for **3f** to −5.92 eV for **3k**. Corresponding LUMO levels, ranging from −1.61 eV (**3f**) to −2.43 eV (**3h**), were determined by taking the optical energy gaps into account, because in the CVs no reduction processes were visible in the potential window of the electrolyte.

Quantum Chemical DFT-Calculations on DTPs

Density functional theory (DFT) calculations were performed on selected DTPs, namely 2′-thienyl-DTP **3b**, *N*-methylpyrrolyl-DTP **3f**, bithienyl-DTP **3h**, 4′-pyridyl-DTP **3k**, 5′-pyrimidyl-DTP **3n**, and for comparison parent phenyl-DTP **3o**, in order to rationalize the electronic and steric in-

fluence of the substituents on the electron density distribution in the frontier molecular orbitals of the neutral and radical cationic species. The results are summarized in Figure 3. As discussed above, it was shown that in alkyl-substituted DTPs the HOMO is only located at the DTP-backbone whereby a node resides at the nitrogen.[5,10] Herein, the same observation was made for the DTPs under investigation and substituents only slightly influenced the HOMO energy level and aromatic electron distribution by inductive effects (Table 3, Figure 3).

On the contrary, the LUMOs extend over the entire molecule, which indicates a quinoidal electron distribution on the DTP unit for all derivatives. An exception can be observed for 5′-pyrimidyl-DTP **3n**, where the LUMO localized exclusively on the pyrimidyl substituent. Time-dependent DFT calculations show a very low oscillator strength for the corresponding CT band and explain their absence in the absorption spectrum.

In the calculated charged species **3b**, **3f**, and **3k**, the electron density distribution of the singly occupied molecular orbitals (SOMOs) is localized on the DTP unit and correlates

	3b (2′-thienyl)	**3f** (N-methyl-pyrrol-2′-yl)	**3h** (5′-bithienyl)	**3k** (4′-pyridyl)	**3n** (5′-pyrimidyl)	**3o** (phenyl)
LUMO	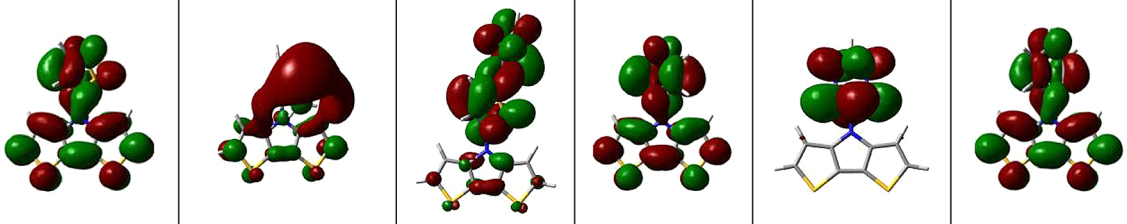					
HOMO	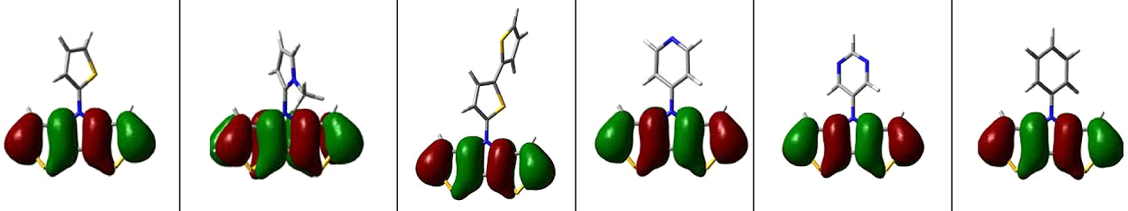					
SOMO	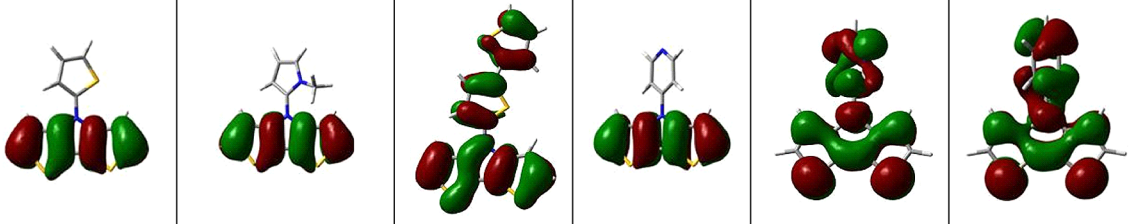					
Torsion angle neutral[a]	47°	91°	46°	37°	41°	43°
Torsion angle charged[a]	22°	26°	17°	43°	59°	58°

Figure 3 Electron density representation of the frontier molecular orbital surfaces of selected neutral and charged DTPs bearing different residues at the nitrogen: 2′-thienyl-DTP **3b**, *N*-methylpyrrolyl-DTP **3f**, bithienyl-DTP **3h**, 5′-pyridyl-DTP **3k**, 5′-pyrimidyl-DTP **3n**, and phenyl-DTP **3o** (from left to right). Molecular orbital surfaces were generated utilizing the Gauss View 5.0 program with an isovalue of 0.02. [a]Twist angle of the substituent at the DTP-nitrogen with respect to the DTP plane.

with the HOMO distribution of the neutral species (Figure 3). In contrast, the electron distribution in the SOMO of the charged species **3h**, **3n**, and **3o** is delocalized over the entire molecule and resembles the HOMO-1 of the neutral molecules.

Furthermore, we calculated the torsion angles of the heteroaromatic substituents versus the DTP plane and obtained values between 37° and 47°. Only, *N*-methylpyrrolyl-DTP **3f** showed an almost perpendicular twist. Upon oxidation, the torsion angles of electron-rich derivatives 2′-thienyl-DTP **3b** (22°), *N*-methylpyrrolyl-DTP **3f** (26°), and bithienyl-DTP **3h** (17°) are significantly reduced and the radical cations flattened. The rather electron-deficient DTPs **3k**, **3n**, and **3o** behave oppositely and their torsion angles are slightly increased after oxidation to angles of 43°, 59°, and 58°, respectively.

Oxidative Polymerization of Selected DTP Derivatives

DTPs have been quite frequently incorporated into conjugated systems, among them are poly(dithienopyrroles) (p(DTP)) and a manifold of co-polymers, which were typically applied in organic solar cells.[3a] P(DTP)s can be best prepared either by chemical or electrochemical oxidation and the resulting conjugated polymers typically show high conjugation length ($\lambda_{max} \approx 550$ nm) and can be easily oxidized. Larger or bulky alkyl substituents at the DTP-nitrogen render them soluble in organic solvents allowing for structural characterization.[5,15]

In this respect, we investigated the electrochemical oxidation of selected heteroarylated DTP-monomers **3b**, **3h**, and **3k**–**3n** in DCM/ACN (1 : 1)/TBAHFP as the electrolyte by potentiodynamic cycling. Thus, the corresponding (semi) conducting polymers p(DTP) **P3b**, **P3h**, and **P3k**–**P3n** were deposited on the platinum working electrode and subsequently characterized in an electrolyte free of monomer (Scheme 2).

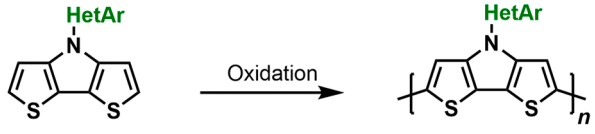

HetAr = 2'-thienyl (**3b**), 5'-bithienyl (**3h**), 4'-pyridyl (**3k**), 2'-pyridyl (**3l**), 2'-pyridimidyl (**3m**), 5'-pyrimidyl (**3n**)

Scheme 2 Electropolymerization of selected DTPs **3** to the corresponding p(DTP)s **P3**.

The evolution of polymer formation is depicted in Figure 4 for all six DTPs investigated. The first scan, which corresponds to the monomer characterization, is plotted in red, the successive nine scans in dark grey. Finally, the electrochemical response and CV of the formed p(DTP), which adheres on the working electrode, are overlaid as a black curve. The first scan in the polymerization experiment, which corresponds to the oxidation of the DTP-monomer **3**, was observed as an irreversible anodic signal in the range of $E_{pa} = 0.55 - 0.87$ V (Table 4). With increasing number of cycles during the polymerization, new redox waves at lower potentials appear and the currents were continuously increasing, because the formed and reactive radical cations undergo coupling at the α-positions and initialize the polymerization according to the well-accepted mechanism for oxidative polymerization of five-membered heterocycles and related monomers such as thiophenes or pyrroles.[16] Dark blue films of conducting p(DTP)s started to form on the surface of the working electrode with increasing number of scans and increasing currents of these signals indicate the growth of the polymer film. After 10 cycles, the electrodes were washed and then subjected to several scans in a monomer-free electrolyte solution until a stable current response was obtained. At this 'conditioning' phase residual oligomeric parts in the film were further polymerized. Subsequently, the polymer films were characterized via CVs applying different scan rates between 10 and 100 mV/s. In all cases, a linear dependency of the corresponding anodic (I_{pa}) and cathodic peak currents (I_{pc}) at different applied scan rates indicated good adherence of the films on the working electrode.

Since the form and shape of CVs of conducting polymers might vary depending on their structure, oxidation and reduction peak potentials are rather diverse. Therefore, more meaningful potential onsets were determined indicating the ease of oxidation of the polymer and the transition from the semiconducting to the conducting state. For our p(DTP)s the onset oxidation potentials were in the range of −0.65 to −0.15 V and in the range of other p(DTP)s.[17] These values are intermediate compared to the well-known PEDOT (−1 V)[18] as an extremely stable polymer in the oxidized conducting state and polythiophenes (PTs) (0.2 V),[19] which are rather stable in the semiconducting state under ambient conditions.[5,15] Corresponding HOMO energies (−4.45 to −4.95 eV) were determined from the onset potentials, which expectedly were substantially raised compared to those of the corresponding monomers due to extended conjugation in the polymers. Finally, we investigated film stabilities by measuring 30 cycles in a defined potential window in order to avoid overoxidation. The losses of electroactivity and exchange of charges were minimal to low and ranged from 0.6% (**P3m**) to 18% (**P3b**). In the case of **P3h** even a slight increase of electroactivity was noted, which we address to further cross-coupling inside the polymer film via the bithiophene sub-

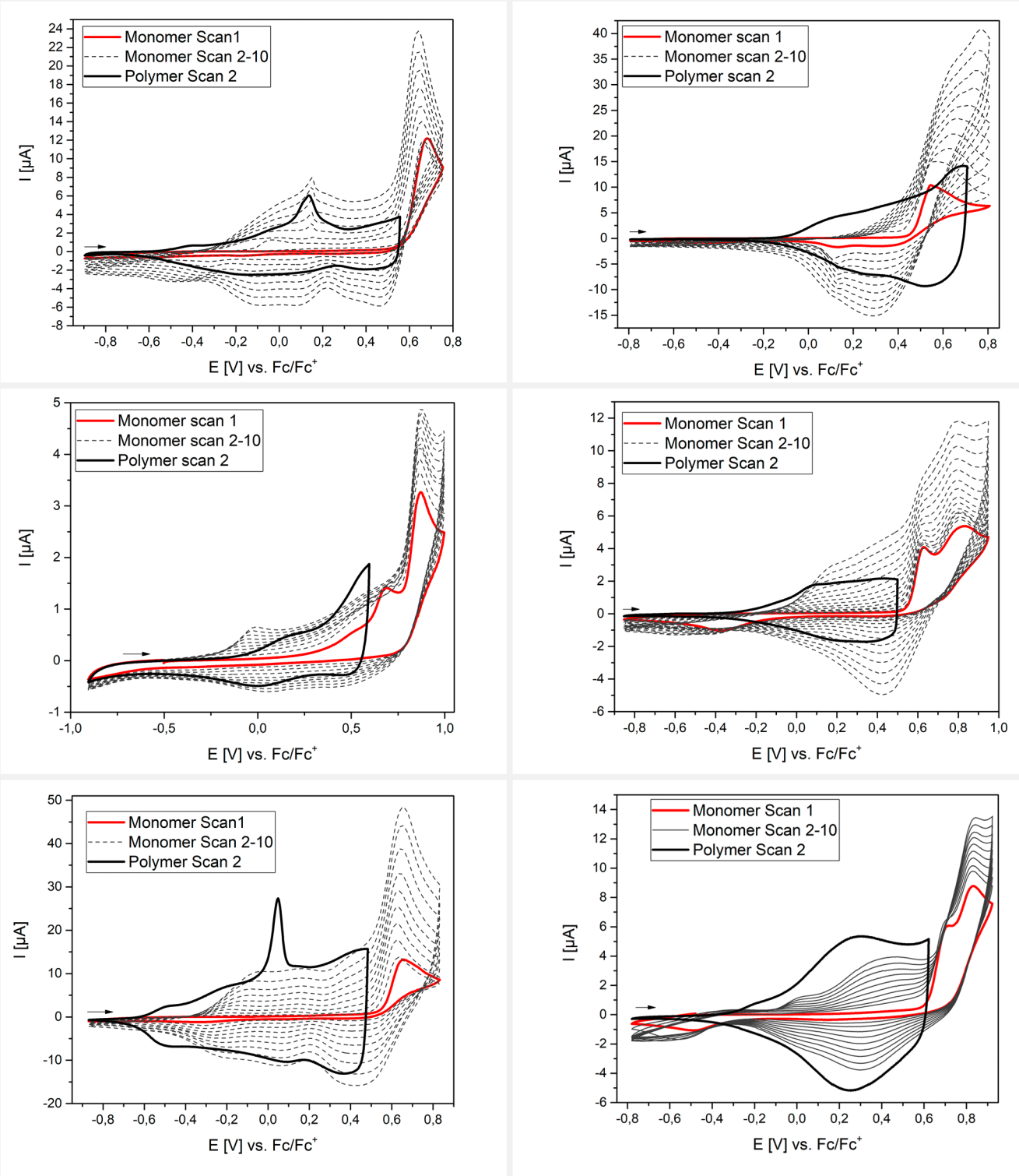

Figure 4 Potentiodynamic polymerization of DTP monomers **3b** (left, top), **3h** (right, top), **3k** (left, middle), **3l** (right, middle), **3m** (left, bottom), and **3n** (right, bottom), in DCM/ACN 1:1 (c = 0.01 M), TBAHFP (0.1 M), 100 mV/s, r.t. The first scan (red) characterizes the oxidation of the monomer, scans 2–10 (dark grey) the continuous growing of the polymer on the working electrode. The CV (Scan 2) of the obtained polymer films **P3** in an electrolyte free of monomer (ACN/TBAHFP 0.1 M, 100 mV/s, r.t.) is shown as black, bold curve.

Table 4 Electrochemical properties of DTPs **3b**, **3h**, and **3k–3n** and corresponding electrochemically prepared polymers p(DTP) **P3b**, **P3h**, and **P3k–P3n** in DCM/ACN 1 : 1, TBAHFP 0.1 M, r. t.

DTP	E_p^{Ox} [V][a]	p(DTP)	E_p^{Ox} [V][a]	E_p^{Red} [V][b]	E_{onset} [V]	E_{HOMO} [eV][c]	Film loss [%][d]
3b	0.68	**P3b**	≈ −0.4/≈ 0.1	≈ 0.15	≈ −0.55	≈ −4.55	18
3h	0.55	**P3h**	≈ 0.1/≈ 0.7	≈ 0.15/≈ 0.5	≈ −0.15	≈ −4.95	0
3k	0.87	**P3k**	≈ 0.2	0.0	≈ −0.25	≈ −4.85	13
3l	0.83	**P3l**	≈ 0.1	0.3	≈ −0.35	≈ −4.75	7.4
3m	0.66	**P3m**	≈ −0.5/≈ 0.0	≈ −0.5/≈ 0.1/≈0.2	≈ −0.65	≈ −4.45	0.6
3n	0.83	**P3n**	≈ 0.3	0.25	≈ −0.35	≈ −4.75	7

Potentials are referenced vs. Fc/Fc^+; [a]E_p^{Ox}: anodic peak potential (scan rate 100 mV/s); [b]E_p^{Red}: cathodic peak potential (scan rate 100 mV/s); [c]redox potential of Fc/Fc^+ is set to −5.1 eV on the Fermi scale; [d]determined as the difference of exchanged charges during scan 2 and scan 30.

stituent. Data for the investigated p(DTP)s are collected in Table 4, and the corresponding additional characterizations are shown in Figures S4 – S9 (SI).

The addition of up to 50 equivalents trifluoroacetic acid to the electrolyte of DTPs **3k** and **3m** only marginally changed potentials. The electrochemical characteristics of the corresponding p(DTP)s **P3k** and **P3m** indicated that protonation equilibria do not play a substantial role for the electrochemical response of the polymers.

Conclusions

In summary, we have presented synthesis of novel N-heteroarylated DTPs **3a–3n** by microwave-assisted Cu-catalyzed coupling of parent *H*-DTP **1** with 5- and 6-membered heteroaromatic halides. Structural characterization of **3a** by single crystal X-ray structure analysis revealed detailed structural information and information about the packing of the molecules in the solid state. The optical and redox properties are dominated by the DTP core and show that the electronic influence of the heterocyclic substituent at the DTP N-atom is rather small. Computational studies revealed a minor influence of the substituents on the HOMO energy level, whereby the LUMO extends over the entire molecule and indicates quinoidal electron distribution. Electrooxidative polymerization of the novel N-heteroarylated DTPs gave electronically well-balanced p(DTP)s, whose onset potentials lie in between those of PEDOT and PTs. Furthermore, the implementation of N-heteroarylated DTPs as a building block into larger oligomers led to novel hole transport materials for perovskite solar cells and is reported as second part of this publication.[20]

Experimental Section

Instruments and Methods

NMR spectra were recorded on an Avance 400 (^{1}H NMR 400 MHz, ^{13}C NMR 101 MHz) or a Bruker AMX 500 spectrometer (^{1}H NMR 500 MHz, ^{13}C NMR 125 MHz). Chemical shifts (δ) are reported in ppm using residual solvent protons (^{1}H NMR: δ_H = 7.26 for $CDCl_3$; δ_H = 3.58 for THF-d_8; ^{13}C NMR: δ_C = 77.2 for $CDCl_3$; δ_C = 67.6 for THF-d_8) as the internal standard. The splitting patterns are designated as follows: s (singlet), d (doublet), t (triplet), and m (multiplet). Coupling constants *J* relate to proton–proton couplings and assignments were made according to the nomenclature numbering scheme. Thin layer chromatography was carried out on aluminum plates, precoated with silica gel, Merck Si60 F254. Preparative column chromatography was performed on glass columns packed with silica gel (particle size 40 – 63 µm) from Macherey-Nagel or aluminium oxide, Merck 90 active basic, particle size 63 – 200 µm. GC-MS measurements were performed on a Shimadzu GCMS-QP2010 SE equipped with an Optima 5MS column (30 m × 0.25 mm) from Macherey-Nagel. High-resolution MALDI mass spectra were recorded on a Bruker SolariX using *trans*-2-[3-(4-*tert*-butylphenyl)-2-methyl-2-propenylidene]malononitrile (DCTB) as a matrix. High-resolution APCI (Atmospheric pressure chemical ionization) spectra were recorded on a Bruker SolariX using ACN as the solvent. For the microwave-assisted synthesis, vials of 10 mL were used in a microwave reactor (CEM Discover, 300 W, 15 bar).

Optical measurements in solution were carried out in 1 cm cuvettes with Merck Uvasol-grade solvents. Absorption spectra were recorded on a Shimadzu UV-3600i Plus UV-vis-nir spectrophotometer. CV experiments were performed with a computer-controlled Autolab PGSTAT30 potentiostat in a three-electrode single-compartment cell (5 mL). The platinum working electrode consisted of a platinum wire sealed in a soft glass tube with a surface of $A = 0.785\ mm^2$, which was polished down to 0.25 µm with Buehler polishing paste prior to use to guarantee reproduci-

ble surfaces. The counter electrode consisted of a platinum wire and the reference electrode was an Ag/AgCl reference electrode. All potentials were internally referenced to the ferrocene/ferricenium couple (Fc/Fc^+). For the measurements, concentrations of 10^{-3} M of the electroactive species were used in freshly distilled and deaerated DCM and ACN (Lichrosolv, Merck) purified with a solvent purification equipment MB-SPS-800 from MBraun. TBAHPF (Sigma-Aldrich, recrystallized twice from ethanol) was applied as the supporting electrolyte in a concentration of 0.1 M and the solution was blanketed with argon during the measurements. For electropolymerizations the respective monomer was used in a concentration of 0.01 M in ACN. The obtained film was washed with dry ACN and subjected to several scans in a monomer-free electrolyte solution until a stable current response was recorded ('conditioning'). Subsequently, the respective film was characterized by CV using different scan rates between 10 and 100 mV/s. At every scan rate two scans were conducted. Additionally, 30 scans were measured with a scan rate of 100 mV/s in order to determine polymer stabilities. The decrease in electroactivity was determined by integrating the second and last scan.

X-ray diffraction data of a colourless plate-shaped single crystal of 3′-thienyl-DTP **3a** were collected in a stream of nitrogen at 150 K on an Agilent SuperNova, Cu at zero, Atlas CCD using graphite-monochromated Cu K_α radiation. Data collection, data reduction, and cell refinement were performed using the CrysAlisPro software.[21] An absorption correction based on the semi-empirical "multi-scan" approach was performed using the SCALE3 ABSPACK scaling algorithm.[21] The structure was solved by charge flipping using Superflip.[22–24] For the final model all non-hydrogen atoms were refined anisotropically using SHELXL.[25]

Quantum chemical calculations were carried out with the Gaussian 09 program.[26] Geometry optimizations and energy calculations were performed via DFT methods using the M06-2X correlation/exchange functional and the 6 – 311+G (d) or the 6 – 311 G basis set. Molecular orbital surfaces were generated utilizing the Gauss View 5.0 program with an isovalue of 0.02.

Materials

Petroleum ether (PE), methanol, and ethyl acetate (EA) were purchased from Avantor. Toluene, DCM, ACN, and THF were purchased from Sigma Aldrich, and dried and purified by an MB SPS-800 solvent purification equipment from MBraun. 3-Bromothiophene **2a** was purchased from Fluorochem. 3-Iodothiophene, 2-bromopyridine **2l**, copper iodide, copper acetate, and copper bromide were purchased from Merck KGaA. 3-Bromofurane **2d** was purchased from OxChem. Magnesium sulfate was purchased from Grüssing GmbH. *N, N*′-Dimethylethylenediamine (DMEDA), 2-bromo-1,3-thiazole **2g**, and potassium phosphate were purchased from Alfa Aesar. 3-Chlorothiophene, 2-bromobenzo[*b*]thiophene **2i**, 2-bromobenzo[*b*]furan **2j**, 4-bromopyridine **2k**, 2-bromopyrimidine **2l**, 5-bromopyrimidine **2n**, and cesium carbonate were purchased from Sigma-Aldrich. 2-Bromothiophene **2b** was purchased from Acros. 2-Bromofurane **2c**,[27] 2-bromoselenophene **2e**,[28] 2-bromo-1-methylpyrrole **2f**,[29] 5-bromo-2,2′-bithiophene **2h**,[30] and 4*H*-dithieno[3,2-*b*:2′,3′-*d*]pyrrole **1**[7] were internally synthesized according to literature-known procedures.

Synthetic Procedures

*General procedure for the reaction of H-DTP **1** with heteroaryl halides **2a–2n** to heteroarylated DTPs **3a–3n**.* In a 10 mL microwave vial equipped with a magnetic stirrer, cesium carbonate (210 mg, 0.64 mmol), copper(I)iodide (11.0 mg, 0.06 mmol), and *H*-DTP **1** (100 mg, 0.54 mmol) were placed and dissolved in 2 mL dry, degassed DMF. After 10 min of stirring at room temperature, 1.2 equiv of the respective heteroaryl halide *2a–n* was added and heated for 45 min at the specified temperature (120–180 °C, 300 W, 15 bar). Subsequently, 20 mL DCM and 20 mL water were added, the phases separated, and the aqueous layer extracted twice with 20 mL DCM. The combined organic phases were washed twice with 20 mL water, dried over magnesium sulfate ($MgSO_4$), filtered, and evaporated. The crude product was purified via column chromatography (LC) to yield the corresponding heteroarylated DTPs.

4-(Thien-3′-yl)-4*H*-dithieno[3,2-*b*:2′,3′-*d*]pyrrole (3a). 3-Bromothiophene **2a** (0.06 mL, 0.66 mmol) or 3-chlorothiophene **2a′** (0.07 mL, 0.71 mmol) or 3-iodothiophene **2a″** (0.08 mL, 0.71 mmol), 160 °C, 45 min. LC: silica gel, PE/DCM 3 : 1; DTP **3a** was isolated as a colourless solid (110 mg, 0.42 mmol, 77%). Mp 111.7–113.4 °C; ^{1}H NMR ($CDCl_3$, 400 MHz): δ = 7.32 (dd, *J* = 5.2, 3.2 Hz, 1 H, $H_{5'}$), 7.23 (dd, *J* = 5.2, 1.5 Hz, 1 H, $H_{4'}$), 7.15 (dd, *J* = 3.2, 1.4 Hz, 1 H, $H_{2'}$), 7.05 (d, *J* = 5.3 Hz, 2 H, H_2), 7.03 (d, *J* = 5.3 Hz, 2 H, H_3) ppm; ^{13}C NMR ($CDCl_3$, 101 MHz): δ = 144.2, 138.4, 126.5, 123.6, 122.6, 116.6, 113.1, 112.3 ppm; HRMS (ESI+): *m/z* $[M + H]^+$, calcd. for $C_{12}H_7NS_3$, 261.9813, found 261.9821, δ*m/m* = 2.86 ppm.

4-(Thien-2′-yl)-4*H*-dithieno[3,2-*b*:2′,3′-*d*]pyrrole (3b). 2-Bromothiophene **2b** (0.06 mL, 0.65 mmol, 1.2 eq); 120 °C, 45 min; LC: silica gel, PE/DCM 3 : 1; DTP **3b** was isolated as a colourless solid (83.0 mg, 0.32 mmol, 58%). Mp 81.6–83.3 °C; ^{1}H NMR ($CDCl_3$, 400 MHz): δ = 7.22 (d, *J* = 5.3 Hz, 1 H, H_2), 7.19 (d, *J* = 5.3 Hz, 1 H, H_3), 7.15 (dd, *J* = 5.5, 1.5 Hz, 1 H, $H_{5'}$), 7.12 (dd, *J* = 3.7, 1.5 Hz, 1 H, $H_{3'}$), 7.06 (dd, *J* = 5.5, 3.7 Hz, 1 H, $H_{4'}$) ppm; ^{13}C NMR ($CDCl_3$, 101 MHz): δ = 144.2, 138.4, 126.5, 123.6, 122.6, 116.6, 113.1, 112.3 ppm; HRMS (APCI): *m/z*

$[M + H]^+$, calcd. for $C_{12}H_7NS_3$, 261.9813, found 261.9819, δ*m*/*m* = 2.02 ppm.

4-(Fur-2′-yl)-4*H*-dithieno[3,2-*b*:2′,3′-*d*]pyrrole (3c). 2-Bromofuran **2c** (95.5 mg, 0.65 mmol); 120 °C, 45 min; LC: silica gel, PE/DCM 85 : 15; DTP **3c** was isolated as a colourless solid (70.0 mg, 0.29 mmol, 52%). Mp 63.1–65.4 °C; ^{1}H NMR ($CDCl_3$, 400 MHz): δ = 7.33 (dd, *J* = 2.0, 1.0 Hz, 1 H, $H_{3'}$), 7.26 (d, *J* = 5.3 Hz, 2 H, H_2), 7.21 (d, *J* = 5.3 Hz, 2 H, H_3), 6.54 (dd, *J* = 3.3, 2.0 Hz, 1 H, $H_{4'}$), 6.17 (dd, *J* = 3.3, 1.0 Hz, 2 H, $H_{5'}$) ppm; ^{13}C NMR ($CDCl_3$, 101 MHz): δ = 147.1, 142.9, 137.6, 123.9, 117.6, 113.1, 111.6, 93.9 ppm; HRMS (APCI): *m*/*z* $[M + H]^+$, calcd. for $C_{12}H_7NOS_2$, 246.0042, found 246.0049, δ*m*/*m* = 2.88 ppm.

4-(Fur-3′-yl)-4*H*-dithieno[3,2-*b*:2′,3′-*d*]pyrrole (3d). 3-Bromofuran **2d** (0.06 mL, 0.65 mmol); 140 °C, 45 min; LC: silica gel, PE/DCM 8 : 2; DTP **3d** was isolated as a colourless solid (92.0 mg, 0.29 mmol, 68%). Mp 73.2–74.8 °C; ^{1}H NMR ($CDCl_3$, 400 MHz): δ = 7.78 (dd, *J* = 1.7, 0.9 Hz, 1 H, $H_{5'}$), 7.55 – 7.53 (m, 1 H, $H_{4'}$), 7.19 (d, *J* = 5.3 Hz, 2 H, H_2), 7.11 (d, *J* = 5.3 Hz, 2 H, H_3), 6.78 (dd, J = 2.0, 0.9 Hz, 1 H, $H_{2'}$); ^{13}C NMR ($CDCl_3$, 101 MHz): δ = 144.4, 143.5, 133.4, 127.6, 123.7, 116.7, 112.0, 106.9 ppm; GC-MS: t_R = 19.3 min, *m*/*z* = 245 (100) $[M]^+$; HRMS (APCI): *m*/*z* $[M + H]^+$, calcd. for $C_{12}H_7NOS_2$, 246.0042, found 246.0048, δ*m*/*m* = 2.32 ppm.

4-(Selenophen-2′-yl)-4*H*-dithieno[3,2-*b*:2′,3′-*d*]pyrrole (3e). 2-Bromoselenophene **2e** (0.14 mg, 0.65 mmol); 120 °C, 45 min; LC: silica gel, PE/DCM 9 : 1; DTP **3e** was isolated as a green oil (86.0 mg, 0.27 mmol, 49%). ^{1}H NMR ($CDCl_3$, 400 MHz): δ = 7.84 (dd with ^{77}Se satellites, ^2J = 23.7 Hz, 1.9 Hz, *J* = 5.7, 1.7 Hz, 1 H, $H_{5'}$), 7.30–7.24 (m, 2 H, $H_{3'}$, $H_{4'}$), 7.25 (d, *J* = 5.4 Hz, 1 H, H_2), 7.20 (d, *J* = 5.3 Hz, 1 H, H_3) ppm; ^{13}C NMR ($CDCl_3$, 101 MHz): δ = 146.3, 145.2, 128.3, 126.7, 123.8, 121.1, 117.3, 112.5 ppm; HRMS (APCI): *m*/*z* $[M + H]^+$, calcd. for $C_{12}H_7NS_2Se$, 309.9257, found 309.9266, δ*m*/*m* = 2.87 ppm.

4-(1-Methylpyrrol-2′-yl)-4*H*-dithieno[3,2-*b*:2′,3′-*d*]pyrrole (3f). 2-Bromo-*N*-methylpyrrole **2f** (104 mg, 0.65 mmol); 140 °C, 45 min; LC: silica gel, PE/DCM 7 : 3; DTP **3f** was isolated as a brown oil (29.0 mg, 0.15 mmol, 27%). ^{1}H NMR ($CDCl_3$, 400 MHz): δ = 7.03 (s, 4 H, H_2, H_3), 6.72 (t, *J* = 2.1 Hz, 1 H, $H_{3'}$), 6.54 (t, *J* = 2.6 Hz, 1 H, $H_{4'}$), 6.26 (dd, *J* = 2.8, 1.9 Hz, 1 H, $H_{5'}$), 3.62 (s, 3 H, H_{CH3}) ppm; ^{13}C NMR ($CDCl_3$, 101 MHz): δ = 146.6, 127.1, 123.6, 120.6, 116.2, 112.1, 107.1, 105.0, 33.0 ppm; HRMS (APCI): *m*/*z* $[M]^+$, calcd. for $C_{13}H_{10}N_2S_2$, 258.0285, found 258.0289, δ*m*/*m* = 1.35 ppm.

4-(1,3-Thiazol-2′-yl)-4*H*-dithieno[3,2-*b*:2′,3′-*d*]pyrrole (3g). 2-Bromothiazole **2g** (0.06 mL, 0.65 mmol); 120 °C, 45 min; LC: silica gel, PE/DCM 95 : 5; DTP **5f** was isolated as a colourless solid (70.0 mg, 0.27 mmol, 48%). Mp 120.1–121.8 °C; ^{1}H NMR ($CDCl_3$, 400 MHz): δ = 7.69 (d, *J* = 5.3 Hz, 2 H, H_2), 7.60 (d, *J* = 3.5 Hz, 1 H, $H_{5'}$), 7.27 (d, *J* = 5.3 Hz, 2 H, H_3), 7.06 (d, *J* = 3.5 Hz, 1 H, $H_{4'}$) ppm; ^{13}C NMR ($CDCl_3$, 101 MHz): δ = 159.8, 142.6, 140.0, 124.2, 119.4, 114.7, 112.5 ppm; HRMS (APCI): *m*/*z* $[M + H]^+$, calcd. for $C_{11}H_6N_2S_3$, 262.9766, found 262.9773, δ*m*/*m* = 2.85 ppm.

4-(2′,2″-Bithien-5′-yl)-4*H*-dithieno[3,2-*b*:2′,3′-*d*]pyrrole (3h). 5-Bromo-2,2′-bithiophene **2h** (158 mg, 0.65 mmol); 120 °C, 45 min; LC: silica gel, PE/DCM 9 : 1; DTP **3h** was isolated as a yellow solid (88.0 mg, 0.27 mmol, 46%). Mp 63.1–65.4 °C; ^{1}H NMR ($CDCl_3$, 400 MHz): δ = 7.25 (dd, *J* = 5.1, 1.2 Hz, 1 H, $H_{5''}$), 7.24 (d, *J* = 5.3 Hz, 1 H, H_2), 7.20 (d, *J* = 5.3 Hz, 2 H, H_3), 7.18 (dd, *J* = 3.6, 1.2 Hz, 1 H, $H_{3''}$), 7.11 (d, *J* = 3.9 Hz, 1 H, $H_{3'}$), 7.05 (dd, *J* = 5.1, 3.6 Hz, 1 H, $H_{4''}$), 7.02 (d, *J* = 3.9 Hz, 1 H, $H_{4'}$) ppm; ^{13}C NMR ($CDCl_3$, 101 MHz): δ = 144.8, 140.28, 136.9, 132.5, 127.9, 124.7, 123.8, 123.8, 122.4, 119.1, 117.3, 112.4 ppm; ^{13}C NMR ($CDCl_3$, 101 MHz): δ = 144.8, 140.28, 136.9, 132.5, 127.9, 124.7, 123.8, 123.8, 122.4, 119.1, 117.3, 112.4 ppm; HRMS (APCI): *m*/*z* $[M + H]^+$, calcd. for $C_{16}H_9NS_4$, 343.9691, found 343.9694, δ*m*/*m* = 1.01 ppm.

4-(Benzo[b]thien-2′-yl)-4*H*-dithieno[3,2-*b*:2′,3′-*d*]pyrrole (3i). 2-Bromobenzo[b]thiophene **2i** (138 mg, 0.65 mmol); 180 °C, 45 min; LC: silica gel, PE/DCM 9 : 1; DTP **3i** was isolated as a colourless solid (57.0 mg, 0.18 mmol, 33%). Mp 135.1–137.2 °C; ^{1}H NMR ($CDCl_3$, 400 MHz): δ = 7.84–7.76 (m, 2 H, $H_{4'}$, $H_{7'}$), 7.48–7.37 (m, 2 H, $H_{5'}$, $H_{6'}$), 7.35 (d, *J* = 5.5 Hz, 2 H, H_2), 7.31 (s, 1 H, $H_{3'}$), 7.23 (d, *J* = 5.4 Hz, 2 H, H_3) ppm; ^{13}C NMR ($CDCl_3$, 101 MHz): δ = 144.5, 141.6, 138.4, 135.7, 125.1, 124.4, 123.9, 123.3, 122.2, 117.8, 113.4, 112.7 ppm; HRMS (ESI+): *m*/*z* $[M + H]^+$, calcd. for $C_{16}H_9NS_3$, 311.9970, found 311.9963, δ*m*/*m* = 2.33 ppm.

4-(Benzo[b]fur-2′-yl)-4*H*-dithieno[3,2-*b*:2′,3′-*d*]pyrrole (3j). 2-Bromobenzofuran **2j** (127 mg, 0.66 mmol); 120 °C, 45 min; LC: silica gel, PE/DCM 8 : 2; DTP **3j** was isolated as a colourless solid (78.0 mg, 0.18 mmol, 48%). Mp 126.8–129.1 °C; ^{1}H NMR ($CDCl_3$, 400 MHz): δ = 7.58–7.45 (m, 2 H, $H_{4'}$, $H_{7'}$), 7.42 (d, *J* = 5.3 Hz, 2 H, H_2), 7.28–7.22 (m, 2 H, $H_{5'}$, $H_{6'}$), 7.23 (d, *J* = 5.3 Hz, 2 H, H_3), 6.47 (d, *J* = 0.9 Hz, 1 H, $H_{3'}$) ppm; ^{13}C NMR ($CDCl_3$, 101 MHz): δ = 151.3, 149.4, 142.3, 129.1, 124.3, 123.7, 123.3, 120.3, 118.7, 113.7, 110.9, 88.4 ppm; HRMS (APCI): *m*/*z* $[M + H]^+$, calcd. for $C_{16}H_9NOS_2$, 296.0198, found 296.0201, δ*m*/*m* = 0.91 ppm.

4-(Pyridin-4′-yl)-4*H*-dithieno[3,2-*b*:2′,3′-*d*]pyrrole (3k). 4-Bromopyridine hydrochloride **2k** (126 mg, 0.66 mmol), and cesium carbonate (Cs_2CO_3) (410 mg, 1.19 mmol); 180 °C, 45 min; LC: silica gel, DCM/methanol 99 : 1; DTP **3k** was isolated as a colourless solid (39.0 mg, 0.15 mmol, 27%). Mp 166.2–168.1 °C; ^{1}H NMR ($CDCl_3$, 400 MHz):

δ = 8.73 (d, *J* = 4.2 Hz, 1 H, $H_{2'}$), 7.54 (d, *J* = 5.1 Hz, 2 H, $H_{3'}$), 7.27 (d, *J* = 5.7 Hz, 2 H, H_2), 7.24 (d, *J* = 5.4 Hz, 2 H, H_3) ppm; ^{13}C NMR ($CDCl_3$, 101 MHz): δ = 151.4, 146.8, 142.9, 124.6, 119.2, 115.8, 112.6 ppm; HRMS (ESI+): *m*/*z* [M + H]$^+$, calcd. for $C_{13}H_8N_2S_2$ 257.0202, found 257.0197, δ*m*/*m* = 2.02 ppm.

4-(Pyridin-2′-yl)-4*H*-dithieno[3,2-*b*:2′,3′-*d*]pyrrole (3l). 2-Bromopyridine **2l** (0.06 mL, 0.66 mmol); 180 °C, 45 min; LC: silica gel, DCM/methanol 99 : 1; DTP **3l** was isolated as a grey oil (37.0 mg, 0.14 mmol, 26%). ^{1}H NMR ($CDCl_3$, 400 MHz): δ = 8.56 (ddd, *J* = 4.9, 1.9, 0.9 Hz, 1 H, $H_{6'}$), 7.81 (ddd, *J* = 8.3, 7.4, 1.9 Hz, 1 H, $H_{4'}$), 7.59 (d, *J* = 5.3 Hz, 2 H, H_2), 7.56 (dt, *J* = 8.3, 0.9 Hz, 1 H, $H_{3'}$), 7.22 (d, *J* = 5.3 Hz, 2 H, H_3), 7.14 (ddd, *J* = 7.4, 4.9, 0.9 Hz, 1 H, $H_{5'}$) ppm; ^{13}C NMR ($CDCl_3$, 101 MHz): δ = 152.1, 149.1, 142.8, 138.6, 123.6, 119.8, 118.9, 114.8, 113.1 ppm; HRMS (ESI+): *m*/*z* [M + H]$^+$, calcd. for $C_{13}H_8N_2S_2$, 257.0202, found 257.0200, δ*m*/*m* = 0.60 ppm.

4-(Pyrimidin-2′-yl)-4*H*-dithieno[3,2-*b*:2′,3′-*d*]pyrrole (3m). 2-Bromopyrimidine **2m** (102 mg, 0.65 mmol); 180 °C, 45 min; LC: silica gel, PE/DCM 1 : 1; DTP **3m** was isolated as a colourless solid (117 mg, 0.54 mmol, 82%). Mp 144.7–146.2 °C; ^{1}H NMR ($CDCl_3$, 400 MHz): δ = 8.71 (d, *J* = 4.8 Hz, 2 H, $H_{4'}$), 8.02 (d, *J* = 5.3 Hz, 2 H, H_2), 7.22 (d, *J* = 5.3 Hz, 2 H, H_3), 7.03 (t, *J* = 4.8 Hz, 1H, $H_{5'}$) ppm; ^{13}C NMR ($CDCl_3$, 101 MHz): δ = 158.4, 157.0, 142.8, 123.1, 120.1, 117.9, 115.9 ppm; HRMS (ESI+): *m*/*z* [M + H]$^+$, calcd. for $C_{12}H_7N_3S_2$, 258.0154, found 258.0155, δ*m*/*m* = 0.30 ppm.

4-(Pyrimidin-5′-yl)-4*H*-dithieno[3,2-*b*:2′,3′-*d*]pyrrole (3n). 5-Bromopyrimidine **2n** (102 mg, 0.65 mmol); 180 °C, 45 min; LC: silica gel, PE/methanol 98 : 2; DTP **3n** was isolated as a colourless solid (59.0 mg, 0.22 mmol, 40%). Mp 188.9–193.2 °C; ^{1}H NMR ($CDCl_3$, 400 MHz): δ = 9.24 (s, 1 H, $H_{2'}$), 9.12 (s, 2 H, $H_{4'}$), 7.32 (d, *J* = 5.3 Hz, 2 H, H_2), 7.23 (d, *J* = 5.4 Hz, 2 H, H_3) ppm; ^{13}C NMR ($CDCl_3$, 101 MHz): δ = 158.9, 155.6, 150.0, 143.0, 135.3, 124.9, 118.9, 111.4 ppm; HRMS (ESI+): *m*/*z* [M + H]$^+$, calcd. for $C_{12}H_7N_3S_2$, 258.0154, found 258.0150, δ*m*/*m* = 1.63 ppm.

Acknowledgment

J. Millan thanks the Universidad de La Rioja for the financial support (EICOD21/01).

Supporting Information

Details on X-ray structure analysis and electrochemical polymerizations are given in the Supporting Information. Supporting Information for this article is available online at https://doi.org/10.1055/a-1972-5895.

Conflict of Interest

The authors declare no conflict of interest.

References

(1) Zhang, X.; Steckler, T. T.; Dasari, R. R.; Ohira, S.; Potscavage, Jr, W. J.; Prakash Tiwari, S.; Coppée, S.; Ellinger, S.; Barlow, S.; Brédas, J.-L.; Kippelen, B.; Reynolds, J. R.; Marder, S. R. *J. Mater. Chem.* **2010**, *20*, 123.
(2) Lu, H.-I.; Lu, C.-W.; Lee, Y.-C.; Lin, H.-W.; Lin, L.-Y.; Lin, F.; Chang, J.-H.; Wu, C.-I.; Wong, K.-T. *Chem. Mater.* **2014**, *26*, 4361.
(3) (a) Rasmussen, S. C.; Evanson, S. J. *Prog. Polym. Sci.* **2013**, *38*, 1773; (b) Ogawa, K. Dissertation, North Dakota State University, **2005**.
(4) Rasmussen, S. C.; Uzelac, E. J.; Culver, E. W. *Adv. Heterocycl. Chem.* **2020**, *10*, 75.
(5) Förtsch, S. PhD thesis, University of Ulm, **2018**.
(6) Gronowitz, S. *Thiophene and its derivatives*. In The Chemistry of Heterocyclic Hompounds; Vol. 44.2; Weissberger, A.; Taylor, E. C. J. Wiley & Sons, New York; **1986**; 631.
(7) Förtsch, S.; Vogt, A.; Bäuerle, P. *J. Phys. Org. Chem.* **2017**, *30*, e3743.
(8) Yin, X.; Zhou, J.; Song, Z.; Dong, Z.; Bao, Q.; Shrestha, N.; Bista, S. S.; Ellington, R. J.; Yan, Y.; Tang, W. *Adv. Funct. Mater.* **2019**, *29*, 1904300.
(9) Cao, J.; Du, F.; Yang, L.; Tang, W. *J. Mater. Chem. A* **2020**, *8*, 22572.
(10) Vogt, A.; Schwer, F.; Förtsch, S.; Lorenz, C.; Mena-Osteritz, E.; Aubele, A.; Kraus, T.; Bäuerle, P. *Chem. Eur. J.* **2021**, *27*, 12362.
(11) Kwon, J. K.; Cho, J. H.; Ryu, Y.-S.; Oh, S. H.; Yum, E. K. *Tetrahedron* **2011**, *67*, 4820.
(12) Wetzel, C.; Brier, E.; Vogt, A.; Mishra, A.; Mena-Osteritz, E.; Bäuerle, P. *Angew. Chem. Int. Ed.* **2015**, *54*, 12334.
(13) Evenson, S. J.; Pappenfus, T. M.; Ruiz Delgado, M. C.; Radke-Wohlers, K. R.; López-Navarrete, J. T.; Rasmussen, S. C. *Phys. Chem. Chem. Phys.* **2012**, *14*, 6101.
(14) Ates, M.; Arican, F.; Karazehir, T. *Bull. Mater. Sci.* **2013**, 36, 1281.
(15) Förtsch, S.; Bäuerle, P. *Polym. Chem.* **2017**, *8*, 3586.
(16) Audebert, P.; Miomandre, F. *Electrochemistry of Conducting Polymers*. In Handbook of Conducting Polymers, 3rd ed.; Skotheim, T. A.; Reynolds J. R. CRC Press: Boca Raton, USA, **2007**; 1.
(17) Förtsch, S.; Mena-Osteritz, E.; Bäuerle, P. *Polym. Chem.* **2021**, *12*, 3332.
(18) Volkov, A. V.; Wijeratne, K.; Mitraka, E.; Ail, U.; Zhao, D.; Tybrandt, K.; Andreasen, J. W.; Berggren, M.; Crispin, X.; Zozulenko, I. V. *Adv. Funct. Mater.* **2017**, *27*, 1700329.
(19) Araujo, R. B.; Banerjee, A.; Panigrahi, P.; Yang, L.; Sjödin, M.; Strømme, M.; Araujo, C. M.; Ahuja, R. *Phys. Chem. Chem. Phys.* **2017**, *19*, 3307.
(20) Almalki, M.; Lorenz, C.; Vogt, A.; Alanazi, A.; Gao, J.; Zakeeruddin, S. M.; Bäuerle, P.; Eickemeyer, F. T.; Grätzel, M. *Org. Mater.* **2023**, *5*, 48.
(21) CryaAlisPro, Agilent Technologies XRD Products.
(22) Palatinus, L.; Chapuis, G. *J. Appl. Crystallogr.* **2007**, *40*, 786.
(23) Palatinus, L.; van der Lee, A. *J. Appl. Crystallogr.* **2008**, *41*, 975.
(24) Palatinus, L.; Prathapa, S. J.; van Smaalen, S. *J. Appl. Crystallogr.* **2012**, *45*, 575.
(25) Sheldrick, G. M. *Acta Crystallogr., Sect. A: Found.* **2008**, 64, 112.
(26) Frisch, M. J. Gaussian, Inc.,: Wallingford, CT, **2013**.

(27) Melas-Kyriazi, J.; Ding, I. K.; Marchioro, A.; Punzi, A.; Hardin, B. E.; Burkhard, G. F.; Tétreault, N.; Grätzel, M.; Moser, J.-E.; McGehee, M. D. *Adv. Energy Mater.* **2011**, *1*, 407.
(28) Wang, Y.-K.; Yuan, Z.-C.; Shi, G.-Z.; Li, Y.-X.; Li, Q.; Hui, F.; Sun, B.-Q.; Jiang, Z.-Q.; Liao, L.-S. *Adv. Funct. Mater.* **2016**, *26*, 1375.
(29) Kim, G.-W.; Choi, H.; Kim, M.; Lee, J.; Son, S. Y.; Park, T. *Adv. Energy Mater.* **2020**, *10*, 1903403.
(30) Pham, H. D.; Yang, T. C.-j.; Jain, S. M.; Wilson, G. J.; Sonar, P. *Adv. Energy Mater.* **2020**, *10*, 1903326.